13th International Symposium on Particle Image Velocimetry – ISPIV 2019
Munich, Germany, July 22-24, 2019

Lagrangian method to characterize interactions of vortices and outer layer flow around a laminar separation bubble

Kai Zhang[1*], **David E. Rival**[1]

[1] Queen's University, Mechanical and Materials Engineering, Kingston, Canada
[*] zhang.kai@queensu.ca

Abstract

This work presents a case study of a SD7003 airfoil to demonstrate the feasibility of a Lagrangian tracking method, which characterizes local flow separation and the interactions between vortices and the outer flow layer around a laminar separation bubble. Two-dimensional time-resolved particle-tracking velocimetry (PTV) is used to measure the laminar separation bubble on the suction side of the SD7003 airfoil. The measurements provide information regarding the separation, transition and reattachment based on the mean velocity and Reynolds stress fields. The flow field is composed of outer and inner flow layers, which are divided by the local minimum velocity magnitude line. Subsequently, extended pathlines are calculated using a technique developed by Rosi and Rival (2018), such that fluid parcels entering the field of interest are tracked continuously. The fluid parcels are labeled according to their trajectories to quantify the entrainment process. No entrainment is observed in the laminar flow region, and the entrainment process is initiated by the formation of vortices near the reattachment point. Particle residence time (PRT) is directly calculated by a technique developed by Jeronimo et al. (2019), and it is shown that an increasing PRT value is induced by the entrainment process.

1 Introduction

Laminar separation bubbles exist at Reynolds numbers of $O(10^4\text{-}10^6)$, and thus a proper characterization of local flow separation is crucial for the prediction and prevention of unsteady loadings on lifting bodies, including low-pressure turbine blades in aircraft engines. During high-altitude operation, the Reynolds number of these turbine blades can decrease to values below $25,000$ (Fernandez et al. (2013)), which can cause severe flow-induced vibration, also referred to as buffeting or flutter . Traditional Eulerian experimental methods (e.g. time-resolved particle image velocimetry (TR-PIV), scanning PIV and tomographic PIV (Tomo-PIV)) have been implemented to examine the flow behaviour of laminar separation bubbles (Burgmann et al. (2008); Zhang et al. (2008); Nati et al. (2015)), however, these measurements cannot account for the interactions between the outer flow layer and vortices in a laminar separation bubble. Rosi and Rival (2018) have developed a Lagrangian method that enables the direct tracking of the enstrophy time history of fluid parcels from the extended flowmap. This new Lagrangian measurement technique provides a new perspective towards studying entrainment, and can therefore be applied to elucidate the interactions between vortices and the outer flow layer in a laminar separation bubble. Jeronimo et al. (2019) further extended this method to directly measure the particle residence time (PRT), which is an indicator of separation and recirculation. The current study exploits the novel Lagrangian measurement techniques described in the previous studies to characterize the interactions between the laminar separation bubble and outer flow layer, to quantify the PRT of each individual fluid parcel, and to demonstrate the feasibility of the presented Lagrangian measurement technique for a variety of flow cases.

2 Experimental method

Fig. 1 shows a schematic of the experimental setup. Experiments were performed in a water-filled, optical towing tank with approximate dimensions of $1 \times 1 \times 15$ m. A traverse system towed a SD7003 airfoil model

with a chordlength $c = 20$ cm at a speed of $U_c = 0.3$ m/s, and the airfoil model was mounted at an angle of attack of $AOA = 8°$. The chordlength based Reynolds number was 60,000. Time-resolved particle-tracking velocimetry (PTV) measurements were performed using a Photron SAZ camera at 4000 Hz with a full resolution of 1024×1024 pixels. Illumination was provided by a high speed laser (Photonics DM40-527), and the light sheet was positioned 25 cm from the tank wall. The tank was seeded with neutrally-buoyant fluorescent particles (Cospheric FMR-1.3, partilce size 1-5 µm). The field of view of the measurement was 28×28 mm, and the scan distance is 160 mm (Fig. 1(b)). The PTV measurements were repeated and recorded 50 times, and the raw images acquired were imported into Davis 8.4.1 (LaVision) and processed using the time-series PTV tracking algorithm.

The short pathlines were then extended beyond their measured length following the method described by Rosi and Rival (2018), which was inspired by flow-map compilation techniques (Raben et al. (2014); Brunton and Rowley (2010)). The pathline-extension method extends paths forwards and backwards in time using flow maps fitted at each time step. Backwards- and forwards-time flow maps were fit using a locally-weighted scatter-plot smoothing algorithm (within MATLAB 2018a) that considered all pathlines that existed at previous or subsequent time steps, respectively. The flow maps contain fit functions for each particle, at every time step, that are generated using the nearest 1.2% of all Lagrangian tracers – approximately 20 particles. Selecting too few tracers for the fitting function yields noisy results, while too many tracers smooths out flow physics. Pathlines were then extended until the beginning or end of the recording, or until they convected out of the field of view according to the flow maps. Pathlines that would extend outside of the field of view were terminated at the periphery. This can occur in backwards- or forwards-time extension and resulted in a small number of nonphysical, erroneous pathlines, particularly evident in the early stages of vortex ring formation ($T < 2$). The resulting pathlines were then smoothed using a third-order Savitzky-Golay filter spanning eleven time steps. Particle residence time (PRT) is then directly measured from the extended pathlines using the method developed by (Jeronimo et al. (2019)).

3 Results and discussion

Fig. 2 shows the instantaneous velocity field from a PTV measurement. The (x,y) coordinates are normalized by the chordlength of the airfoil and denote the streamwise and vertical directions, respectively. An average of 1200 fluid parcels were tracked at each time step and produced pathlines with a mean length of four time steps. The origin of the field is located at the leading edge of the airfoil, and the velocity is normalized by the towing speed. As revealed in Fig. 2, the PTV measurement captures the dynamics of the laminar separation bubble. Fig. 2(a) shows that the flow is still attached to the leading edge of the airfoil, and Fig. 2(b) reveals that flow separation occurs near $x/c = 0.05$. Subsequently, an elongated vortex is observed at the end of the laminar separation bubble in Fig. 2(c). This vortex sheds from the laminar separation bubble and forms a circular vortex further along the length of the airfoil, which is shown in Fig. 2(d).

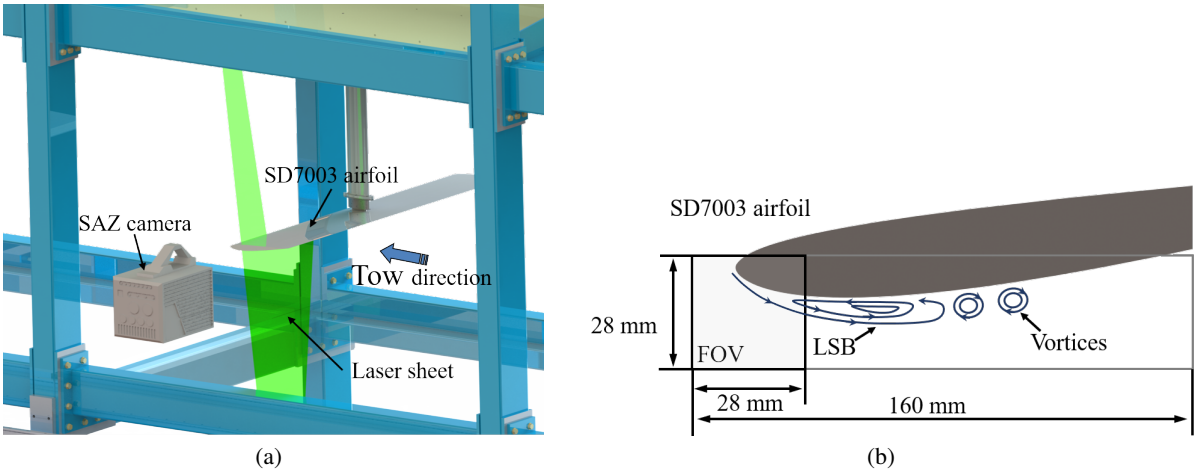

Figure 1: **(a)** Experimental setup and PTV measurement system; **(b)** Schematic of the SD7003 airfoil, measurement field of view and scanning distance for the PTV measurements.

By interpolating the instantaneous PTV tracking results into a rectilinear grid spacing of $x/c = 0.0025$, the ensemble-average was performed to obtain the mean velocity and Reynolds stress. With the same coordinate system as described above, Fig. 3(a) displays the normalized streamwise velocity. The separation point is defined as the location where the near-wall mean velocity is $U^* = 0$, which is located at $x/c = 0.06$. Due to the vortices formed at the backside of the laminar separation bubble, it is relatively difficult to determine the reattachment point. Following the method described in Ol et al. (2005), the reattachment point is the location where the near-wall velocity magnitude increases, which is $x/c = 0.22$. Fig. 3(b) reveals the distribution of the Reynolds stress, where values of $u'v'^* < 0.001$ are shown. The transition point where the Reynolds stress begins to increase is clearly shown at $x/c = 0.146$. The peak Reynolds stress observed in Fig. 3(b) is caused by the onset of vortex shedding.

The obtained separation, transition and reattachment points that were measured in this study match the experimental results in the existing literature (Ol et al. (2005)). However, the Eulerian plots shown in Figs. 3(a) and (b) are limited since they are unable to reveal the interactions between the laminar separation bubble and the outer flow layer. Thus, new Langrangian measurement techniques (Rosi and Rival (2018); Jeronimo et al. (2019); Zhang et al. (2019) (2019)) are implemented to elucidate the interactions between the laminar separation bubble and the outer flow layer. First, we divided the flow field into inner and outer layers, which are separated by the minimum velocity magnitude line shown in Fig. **??**. The first portion of the minimum velocity magnitude line ($0.05 < x/c < 0.15$) represents the centreline of the shear layer between the outer flow layer and the laminar separation bubble. The remaining portion of the minimum velocity magnitude line denotes the mean vortex core trajectory of the shedding vortices.

The field of interest used in this study was selected to ensure that the entire vortex could be observed during the experiments. The backside vortices that propagate downstream remain two-dimensional until $x/c = 0.35$, at which point three-dimensional instability is initiated. The field of interest used in this study ranges from $0 < x/c < 0.35$ and $-0.02 < y/c < 0.08$, as shown in Fig. **??**. Using the pathline extension method described in the experimental setup section, the pathlines of the fluid parcels that enter the field of interest are extended forwards until they convect out of the field of interest or the extended parcel location surpasses the boundary of the measurement windows at the local time step. The red fluid parcels are tagged to indicate those that enter the field of interest within the entrance region (red dash box in Fig. 2(a)) and remain in the outer flow layer, while blue fluid parcels also enter the field of interest within the entrance region, but convect into the inner flow layer. Fig. 4(b) shows that both the red and blue parcels follow the minimum velocity magnitude line before the transition point. This demonstrates that the shear layer remains stable in the laminar region, and thus continues to divide the laminar separation bubble and the outer flow layer. Consequently, no interaction between the two flow layers is observed. In Fig. 4(c), it is shown that the inner and outer flow layers interact through the formation of vortices near the reattachment point. Subsequently, Fig. 4(d) shows that the blue fluid parcels are entering the inner flow layer, which are then propagated downstream by the shedding vortices.

The particle residence time (PRT) value of each fluid parcel is calculated using the method developed by (Jeronimo et al. (2019)). The PRT value is defined as the amount of time, t_p, that a fluid parcel remains inside of the field of interest, which is normalized by the chordlength and towing speed of the airfoil ($\text{PRT} = t_p U_c/c$). The contour plots in Fig. 5(a) display the PRT values of each fluid parcel. It is shown in Fig. 5(a) that the PRT value monotonically decreases in the y-direction. The region with the highest PRT value corresponds to the fluid parcels that are closest to the laminar separation bubble. Fig. 5(b)-(d) reveal that the fluid parcels that compose the shedding vortices in the vortex core possess the highest PRT value.

Fig. 6 shows the average particle residence time for five sub-fields of interest (green dashed boxes in the inset of Fig. 6. Each sub-field has a width of $x/c = 0.05$, spanning a range of $0 < x/c < 0.25$. The red rectangular and blue triangular markers shown in Fig. 6 correspond to the average PRT values for both the red and blue fluid parcels, respectively, which are shown in Fig. 5. The red and blue fluid parcels in the first three sub-fields of interest have relatively similar mean PRT values, however, such values for blue fluid parcels increase significantly past the transition point, while the PRT values for the red fluid parcels remain unchanged. It is observed from this plot that the formation of vortices increases the mean PRT value.

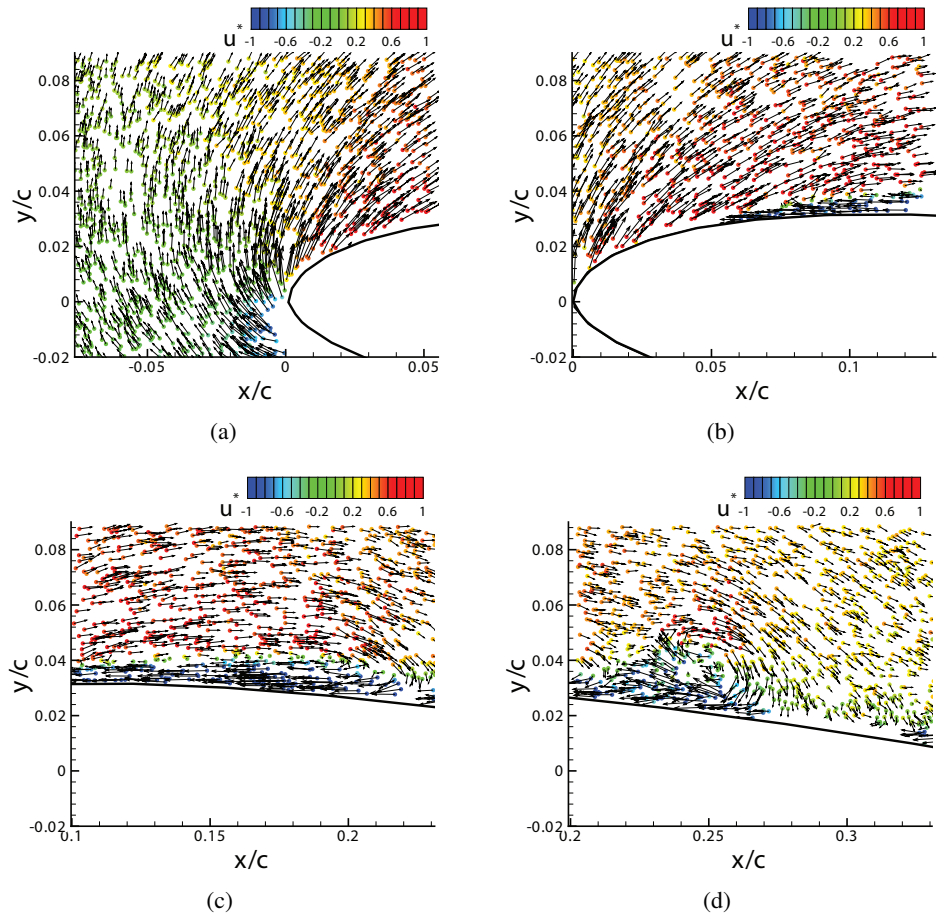

Figure 2: Instantaneous tracer position and velocities captured by PTV measurment.

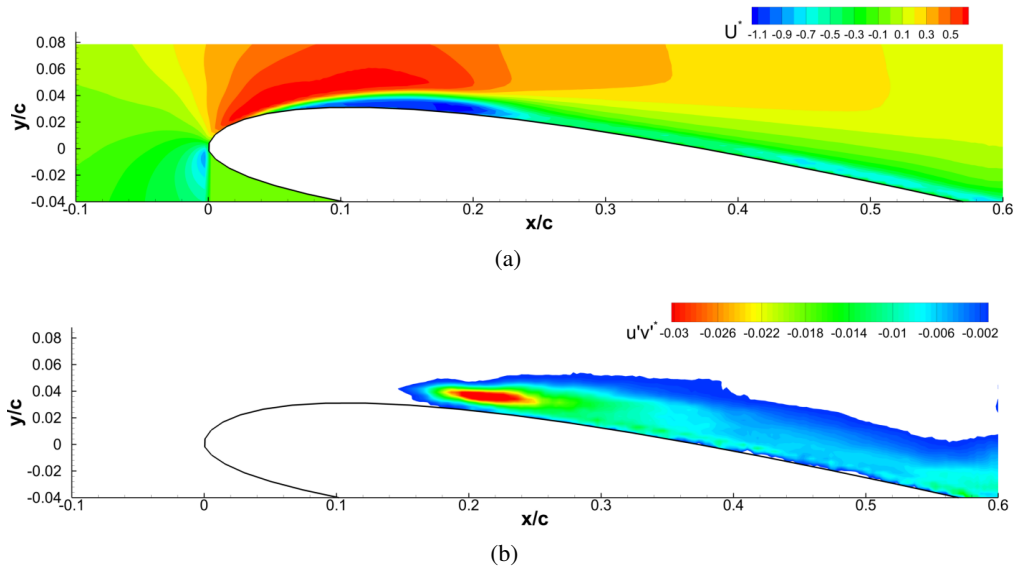

Figure 3: Ensemble-average velocity and Reynolds stress fields.

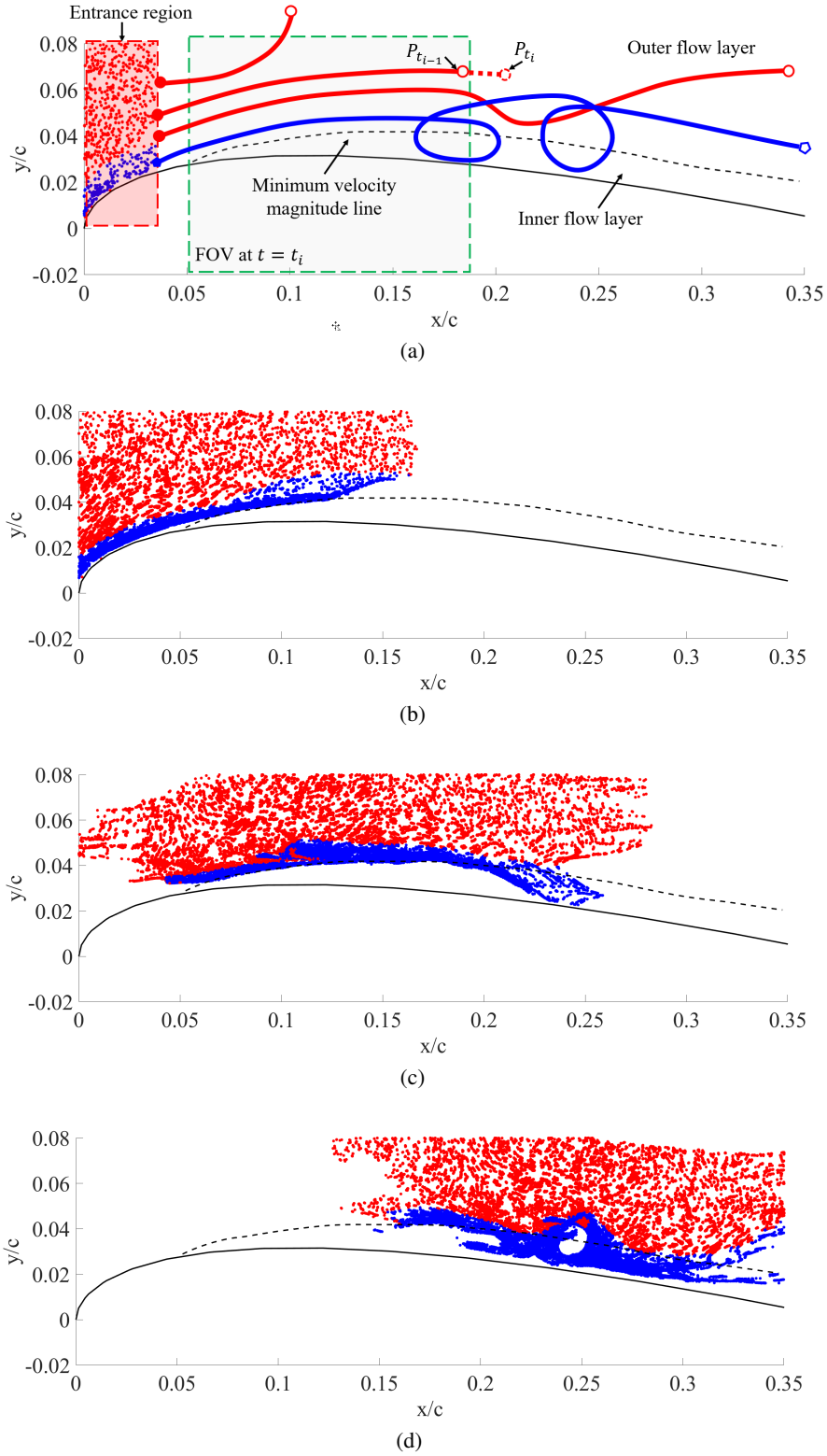

Figure 4: **(a)** Schematic of extended pathlines and fluid parcel tagging method. Fluid parcels are coloured according to their source and trajectory. Red fluid parcels enter the field of interest from the entrance region but do not enter the inner flow layer. Blue fluid parcels enter the field of interest from the entrance region and enter the inner flow layer; **(b)-(d)** Instantaneous tagged fluid parcel locations for different time steps.

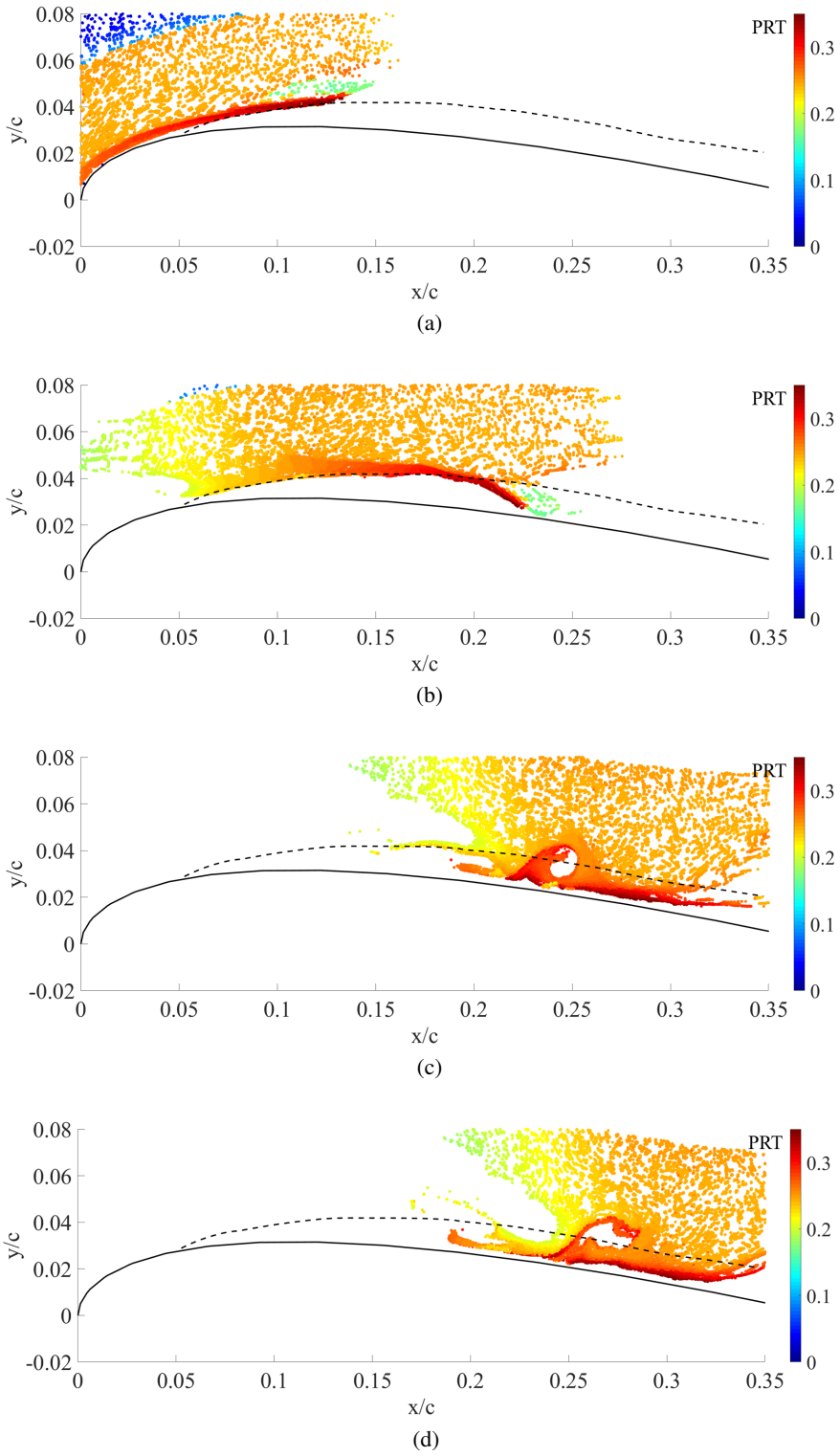

Figure 5: PRT value of each fluid parcel at different time steps.

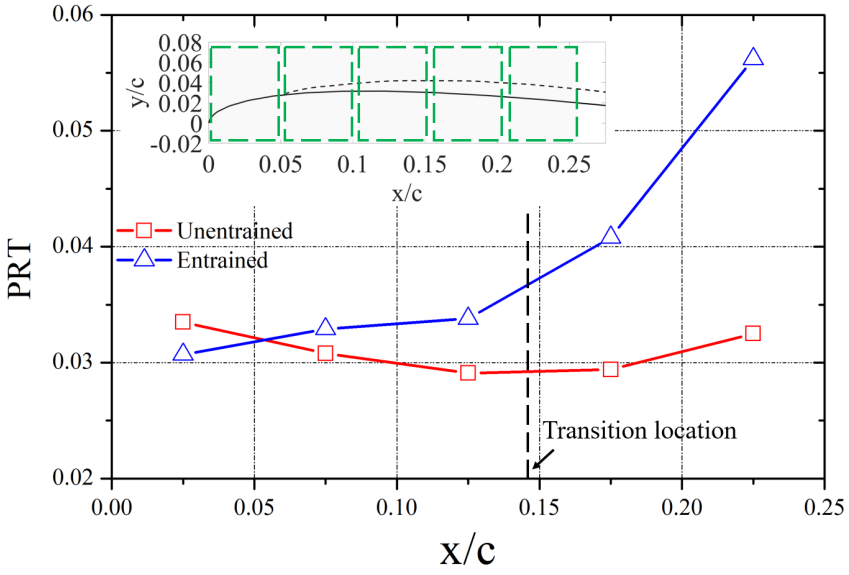

Figure 6: Mean PRT values within five different sub-fields of interest for entrained and unentrained fluid parcels.

4 Conclusions

The current study examines the behavior of a laminar separation bubble over a SD7003 airfoil using a new Lagrangian tracking method. Spatially and temporally-resolved 2D-PTV measurements were performed to reveal the flow fields near the laminar separation bubble. The laminar separation bubble and the vortices at the backside of the bubble (towards the trailing edge of the airfoil) were reconstructed using the instantaneous results. The separation, transition and reattachment points were captured by the time-averaged velocity and Reynolds stress measurements.

A pathline extension method described in Rosi and Rival (2018) was performed to track each fluid parcel that entered the field of interest. The field of interest ranges $0 < x/c < 0.35$, which covered the entire laminar separation bubble. The flow field is divided into two regions defined by the minimum velocity magnitude line: one region is the outer flow layer and the other is the layer influenced by flow separation, which is referred to as the inner flow layer. The vortices at the backside of the laminar separation bubble play a crucial role in the interactions between the two flow layers. It is shown that the laminar separation bubble is isolated from the outer flow layer in the laminar flow range, and the formation of vortices causes the fluid parcels from the outer flow layer to cross the minimum velocity magnitude line.

The particle residence time (PRT), pertinent to the aforementioned field of interest, is directly calculated by tracking and extending particle trajectories (Jeronimo et al. (2019)). The PRT value of the incoming fluid parcels is a clear indicator of break of the laminar separation bubble. The PRT value of the fluid parcels corresponding to the outer flow layer remained relatively constant over the transition and reattachment points, while the fluid parcels that interact with the inner flow layer have an increasing PRT value once they pass the aforementioned points.

The new Lagrangian measurement technique presented in this work is particularly important for elucidating the dynamics of laminar separation bubbles and the entrainment of the outer flow layer. Accurate measurements of these complex flows will improve our understanding of laminar separation bubbles, and will provide insight into enhancing the stability and performance of low-pressure turbines in aircraft engines. The presented measurement technique can therefore be implemented in other challenging flow cases.

Acknowledgements

The authors would like to acknowledge the support from a Natural Sciences and Engineering Research Council (NSERC) CRD grant in partnership with Pratt & Whitney Canada.

References

Brunton SL and Rowley CW (2010) Fast computation of FTLE fields for unsteady flows: a comparison of methods. *Chaos* 20:17503

Burgmann S, Dannemann J, and Schröder W (2008) Time-resolved and volumetric piv measurements of a transitional separation bubble on an sd7003 airfoil. *Experiments in Fluids* 44:609–622

Fernandez E, Kumar R, and Alvi F (2013) Separation control on a low-pressure turbine blade using micro-jets. *Journal of Propulsion and Power* 29:867–881

Jeronimo MD, Zhang K, and Rival DE (2019) Direct lagrangian measurements of particle residence time. *Experiments in Fluids* 60:72

Nati A, De Kat R, Scarano F, and Van Oudheusden B (2015) Dynamic pitching effect on a laminar separation bubble. *Experiments in Fluids* 56:172

Ol M, McCauliffe B, Hanff E, Scholz U, and Kähler C (2005) Comparison of laminar separation bubble measurements on a low reynolds number airfoil in three facilities. in *35th AIAA fluid dynamics conference and exhibit*

Raben SG, Ross SD, and Vlachos PP (2014) Computation of finite-time Lyapunov exponents from time-resolved particle image velocimetry data. *Experiments in fluids* 55:1638

Rosi GA and Rival DE (2018) A Lagrangian perspective towards studying entrainment. *Experiments in Fluids* 59:19

Zhang K, Rival DE, and Jeronimo M (2019) Lagrangian method to visualize transport behavior of liquid and solid phases: Feasibility study in a confinement vortex ring. *Submitted to Experiments in Fluids*

Zhang W, Hain R, and Kähler CJ (2008) Scanning piv investigation of the laminar separation bubble on a sd7003 airfoil. *Experiments in Fluids* 45:725–743